Neuron, Vol. 44, 947–960, December 16, 2004, Copyright ©2004 by Cell Press

Axon Sorting in the Optic Tract Requires HSPG Synthesis by *ext2* (*dackel*) and *extl3* (*boxer*)

Jeong-Soo Lee,[1] Sophia von der Hardt,[2] Melissa A. Rusch,[3] Sally E. Stringer,[3] Heather L. Stickney,[4] William S. Talbot,[4] Robert Geisler,[2] Christiane Nüsslein-Volhard,[2] Scott B. Selleck,[3] Chi-Bin Chien,[1,6,*] and Henry Roehl[2,5,6]

[1]Department of Neurobiology and Anatomy
University of Utah
20 North 1900 East
Salt Lake City, Utah 84103
[2]Abteilung Genetik
MPI für Entwicklungsbiologie
Spemannstrasse 35/III
D-72076 Tübingen
Germany
[3]Departments of Pediatrics and Genetics
Cell Biology and Development
University of Minnesota
Minneapolis, Minnesota 55455
[4]Department of Developmental Biology
Stanford University School of Medicine
Stanford, California 94305
[5]Centre for Developmental
and Biomedical Genetics
Department of Biomedical Science
University of Sheffield
Sheffield S10 2TN
United Kingdom

Summary

Retinal ganglion cell (RGC) axons are topographically ordered in the optic tract according to their retinal origin. In zebrafish *dackel* (*dak*) and *boxer* (*box*) mutants, some dorsal RGC axons missort in the optic tract but innervate the tectum topographically. Molecular cloning reveals that *dak* and *box* encode *ext2* and *extl3*, glycosyltransferases implicated in heparan sulfate (HS) biosynthesis. Both genes are required for HS synthesis, as shown by biochemical and immunohistochemical analysis, and are expressed maternally and then ubiquitously, likely playing permissive roles. Missorting in *box* can be rescued by overexpression of *extl3*. *dak;box* double mutants show synthetic pathfinding phenotypes that phenocopy *robo2* mutants, suggesting that Robo2 function requires HS in vivo; however, tract sorting does not require Robo function, since it is normal in *robo2* null mutants. This genetic evidence that heparan sulfate proteoglycan function is required for optic tract sorting provides clues to begin understanding the underlying molecular mechanisms.

*Correspondence: chi-bin.chien@neuro.utah.edu
[6]These authors contributed equally to this work.

Introduction

Topographic projections are critical for sensory processing, and mechanisms that determine the topographic order of axon terminals have been studied intensively, especially in the vertebrate visual system (Udin and Fawcett, 1988). Retinal ganglion cell (RGC) axons form an order-preserving projection between the retina and the tectum, both of which are patterned along anterior-posterior and dorsal-ventral axes. Gradients of guidance receptors along both retinal axes are thought to recognize gradients of tectal ligands (McLaughlin et al., 2003). However, even before reaching the optic tectum, retinal axons are already presorted en route. RGC axons are topographically arranged in the optic nerve as they exit the eye, and after crossing the optic chiasm they undergo a complex rearrangement to yield a new, still topographic, ordering in the optic tract (Scholes, 1979; Straznicky et al., 1979; Chan and Guillery, 1994; Leung et al., 2003). In contrast to the mechanisms of tectal topography, which have been intensively studied, the mechanisms that control sorting in the optic tract have remained essentially unknown.

To elucidate the mechanisms of retinal axon tract sorting, we have taken a genetic approach using the zebrafish visual system. Axons from the dorsal and ventral retina are reliably segregated in the ventral and dorsal brachia, respectively, of the optic tract, and can be easily visualized in whole mounts (Stuermer, 1988; Figure 1). A large-scale screen for retinotectal projection defects identified three complementation groups with defects in optic tract sorting: *boxer* (*box*), *dackel* (*dak*), and *pinscher* (*pic*) (Trowe et al., 1996). Interestingly, all three mutants also show defects in fin and branchial arch development (van Eeden et al., 1996; Schilling et al., 1996), suggesting that they act in a common developmental pathway with reiterated roles. Here, we have molecularly cloned *dak* and *box*, which encode the zebrafish exostosin genes *ext2* and *extl3*, respectively, and analyze their roles in optic tract sorting.

Exostosin family proteins are glycosyltransferases that synthesize the glycosaminoglycan (GAG) chains of heparan sulfate (HS) proteoglycans (HSPGs). These GAG chains are composed of a tetrasaccharide linker (Xyl-Gal-Gal-GlcA) common to both HSPGs and chondroitin sulfate proteoglycans (CSPGs), followed by HSPG-specific chains consisting of repeating glucuronic acid-N-acetylglucosamine (GlcA-GlcNAc) disaccharides of variable lengths (Figure 3E). The vertebrate exostosin family comprises the exostosin genes *Ext1* and *Ext2* and the exostosin-like genes *Extl1*, *Extl2*, and *Extl3* (reviewed in Zak et al., 2002, and references therein). Although the *ext* genes are highly conserved during evolution, only *ext1*, *ext2*, and *extl3* orthologs exist in *Drosophila* (Bornemann et al., 2004; Han et al., 2004; Takei et al., 2004), and only *ext1* and *extl3* exist in *C. elegans* (Kitagawa et al., 2001; Morio et al., 2003). In humans, mutations in either *EXT1* or *EXT2* produce benign tumors at the growth plates of endochondral bone (reviewed in Duncan et al., 2001), and in *Drosophila*

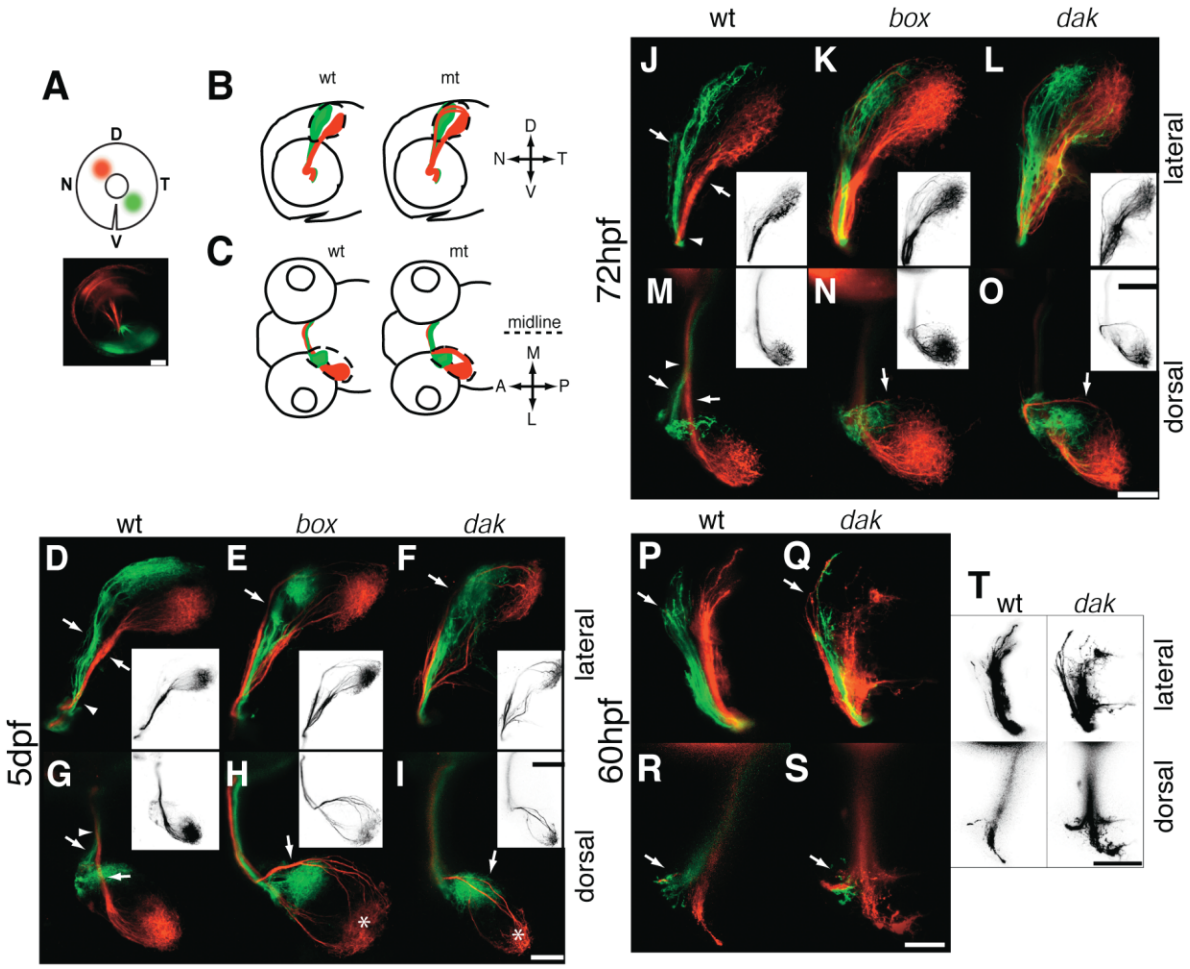

Figure 1. Optic Tract Sorting in wt, *box*, and *dak*

(A) Labeling scheme. Schematic shows injection of DiO (green) into ventrotemporal (VT) eye and DiI (red) into dorsonasal (DN) eye. Lateral view of injected eye shows RGC axons gathering into the optic nerve head. (B and C) Diagrams of wt and mutant tract sorting in lateral (B) and dorsal (C) views. (D–I) Typical projections at 5 dpf. In wt (D and G), DN and VT axons cross over each other shortly after the midline (arrowheads) and are sorted perfectly in the optic tract (arrows). In mutants, VT axons (green) sort and target correctly, but DN axons (red) missort in the optic tract (arrows in [E], [F], [H], and [I]) but then target topographically on the tectum (asterisks in [H] and [I]). (J–O) Typical projections at 72 hpf. Crossing over (arrowheads in [J] and [M]) and sorting of DN axons in wt are already clear at this stage (arrows in [J] and [M]), whereas axons in mutants make clear missorting errors (arrows in [K], [L], [N], and [O]). (P–T) At 60 hpf, wild-types are well sorted but occasionally have single missorted axons (arrows), while *dak* show clear phenotypes with multiple missorted axons (arrows). Insets in (D)–(O) and (T) show DiI labeling as black on white. Alleles: box^{tm70g}, dak^{to273b}. All embryos are shown in both lateral and dorsal views. Scale bars, 50 μm; scale bars in insets, 100 μm. D, dorsal; V, ventral; N, nasal; T, temporal; A, anterior; P, posterior; M, medial; L, lateral; wt, wild-type; mt, mutant.

the exostosin genes *tout-velu* (*ttv*, the *ext1* ortholog), *sister of tout-velu* (*sotv*, *ext2*), and *brother of tout-velu* (*botv, extl3*) are required for morphogen signaling in a number of developmental contexts (reviewed in Nybakken and Perrimon, 2002; Bornemann et al., 2004; Han et al., 2004; Takei et al., 2004). In mouse, *Ext1* is essential for early embryonic patterning (Lin et al., 2000), and brain-specific knockout studies have shown its role in CNS assembly (Inatani et al., 2003). A number of biochemical studies have established Ext1 and Ext2 as heparan sulfate copolymerases in both vertebrate and invertebrate organisms (Zak et al., 2002), and in vitro activities of a *Drosophila* Extl3 homolog encoded by *brother of tout-velu* (*botv*) also suggest the involvement of the Extl proteins in HS formation (Kim et al., 2002). The precise biosynthetic functions of these genes in vertebrates is, however, not established and is of some importance given their critical roles in developmental patterning and tumor formation.

Here, we provide evidence to show that mutations in *ext2* and *extl3* are responsible for missorting of RGC axons in the optic tract. First, *ext2* is very tightly linked to *dak*, and *extl3* is tightly linked to *box*. Second, allelic sequencing reveals nonsense and missense mutations responsible for the *dak* and *box* mutations. Third, heparan sulfate biosynthesis in *dak* and *box* is dramatically reduced, as predicted from the in vitro enzymatic activities of Ext2 and Extl3. Fourth, *ext2* and *extl3* expression patterns and the distribution of HS during embryogenesis, though broad, are consistent with roles in retinotectal pathfinding. Finally, *box* mutant phenotypes are rescued by injection of wild-type *extl3* mRNA. The reti-

notectal defects in both mutants are strikingly specific, with apparently normal brain patterning and axon scaffold formation. These results provide clues to the molecular basis of optic tract sorting, by showing that HSPGs play a required role.

Further, we test genetically whether HSPGs are acting in concert with Slit-Robo signaling, as concluded in several recent studies in which HSPGs were found to play roles in axon guidance (Inatani et al., 2003; Bülow and Hobert, 2004; Johnson et al., 2004; Steigemann et al., 2004). We find that *astray* (*robo2*) mutants have properly sorted tracts, showing that tract sorting does *not* require Slit-Robo signaling. However, *dak;box* double mutants, predicted by our data to have lower HS than either single mutant, display not only tract missorting defects, but also retinal pathfinding defects that are strikingly reminiscent of *astray*, consistent with previous data showing that HS is important for Slit-Robo signaling (e.g., Hu, 2001). Our analysis thus suggests two distinct roles for HS in retinal axon guidance. First, *sorting* of dorsal axons within the optic tract requires a relatively high level of HS but does not require Robo function. Second, *pathfinding* to the tectum (i.e., keeping axons within the optic tract) requires a lower threshold of HS, as well as Robo2 function.

Results

A Subset of Dorsal RGC Axons Missort in *dak* and *box*

In the optic tract, axons from the dorsal retina are sorted in the ventral brachium (or branch), and axons from ventral retina are sorted in the dorsal brachium (wt in Figures 1A–1C). This ordering differs from that seen as axons exit the retina, where they are sorted according to their circumferential position in the retina. Achieving the final ordering found in the tract requires a complex rearrangement of retinal axon fascicles shortly after crossing the optic chiasm (Scholes, 1979). In double-labeled specimens, this rearrangement can be seen as the point where dorsal and ventral axons cross over each other (arrowheads in Figures 1D, 1G, 1J, and 1M). In wild-types, this segregation is very clear at 5 days postfertilization (dpf) (Figures 1D and 1G) and can be observed as early as 60 hr postfertilization (hpf) (Figures 1P, 1R, and 1T). Since axons first reach the tectum at 48 hpf (Stuermer, 1988), this suggests that axons are already sorted as they first grow to the tectum. Further evidence that sorting is an active process is provided by the zebrafish optic tract sorting mutants, which affect this process specifically (Trowe et al., 1996). In *box* and *dak*, a subset of dorsal RGC axons misroute and enter the tectum through the dorsal, instead of the ventral, brachium (Figure 1). This is best seen from a lateral view (Figures 1D–1F and 1J–1L). The phenotype is strong and specific at 5 dpf: ventral axons are unaffected, and many dorsal axons are sorted properly (Figures 1D–1I). This phenotype is seen in *dak* at 60 and 72 hpf (Figures 1L, 1O, 1Q, and 1S) and is occasionally seen in *box* at 72 hpf (Figures 1K and 1N), indicating that missorting occurs early in *dak* and only later in *box*.

In order to quantitate missorting, we topographically labeled eyes in the dorsonasal quadrant. We verified the precision of labeling by checking that the axons terminated in ventroposterior tectum and, when necessary, imaging the eye from a lateral view (Figure 1A). We then developed a missorting index (MI) as a measure of the fraction of missorted dorsonasal axons seen in confocal z stacks (Figure 2A; see Experimental Proce-

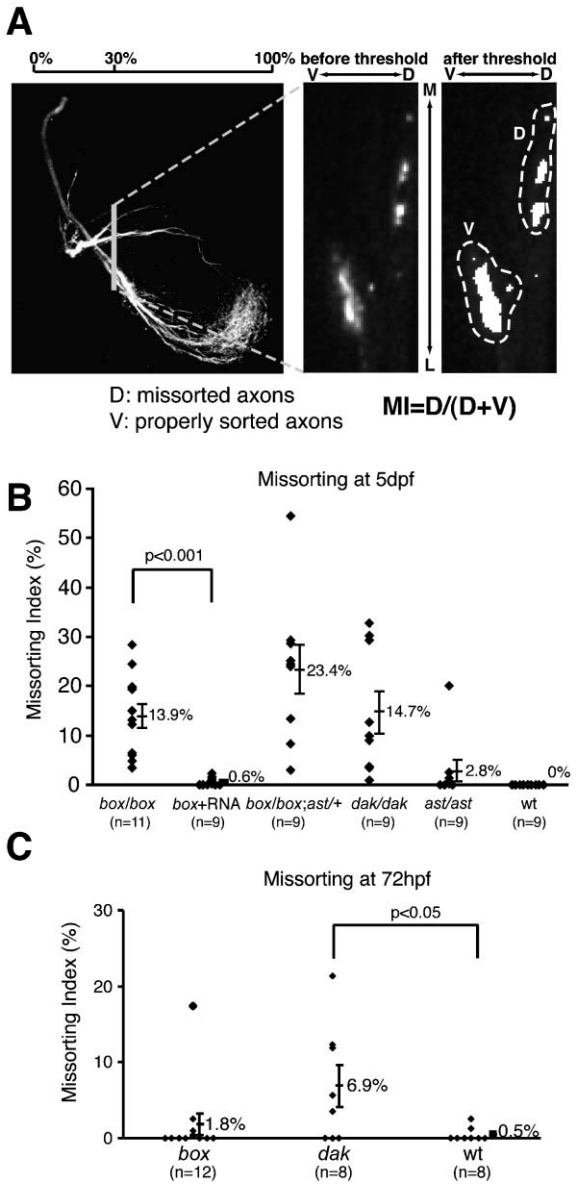

Figure 2. Quantification of Sorting Errors

(A) Calculation of missorting index (MI). After dorsonasal retina was labeled, a dorsal view confocal stack was resliced in the optic tract as shown. The areas occupied by properly sorted ("V") versus missorted axons ("D") were measured using ImageJ (see Experimental Procedures), and the MI was calculated as D/(D + V).

(B) Missorting in mutants at 5 dpf. In wt, dorsal axons are sorted perfectly; in *box*^{tm70g} and *dak*^{to273b}, dorsal axons consistently missort. Missorting in *box* is corrected by *extl3* RNA injection. *ast*^{ti272z} homozygotes show essentially normal sorting, while *box;ast/+* double mutants show mild enhancement compared to *box*.

(C) Missorting at 72 hpf. Missorting is already evident at 72 hpf in *dak*, but only weakly in *box*. There is weak missorting even in wt, suggesting that initially missorted axons are later corrected by 5 dpf.

dures). In 5 dpf wild-types, essentially no axons missorted (MI = 0.0; Figure 2B), but significant numbers of *box* and *dak* axons missorted (MI 13.9%, 14.7%; Figure 2B). At 72 hpf (Figure 2C), a significant fraction of *dak* axons missorted (MI 6.9%), but the missorting in *box* (MI 1.8%) was not significantly different than wild-type. Interestingly, wild-type larvae showed a small number of missorted axons at 72 hpf (MI 0.5%). Missorting in wild-types appeared even more common at 60 hpf: six out of ten wild-type embryos showed missorted axons (e.g., Figures 1P, 1R, and 1T), although the small number of axons precluded meaningful MI measurements. These missorted axons may somehow be corrected during later development. Missorting in *dak* at 60 hpf appeared stronger than wild-type: eight out of ten embryos showed missorting, with several missorted axons per embryo, compared to the one or two missorted axons usually found in wild-type. Despite being missorted in the tract, misrouted axons in mutants eventually make topographically correct terminations in the tectum, implying that these RGCs have not lost their positional identity within the retina (Figures 1H and 1I). In confirmation, in situ hybridization with a battery of dorsal- and ventral-specific retinal markers showed no differences in eye patterning between *box* and wild-type (*tbx5*, *raldh2*, and *vax2*; data not shown). The specific phenotypes of *dak* and *box* in optic tract sorting show that tract sorting and tectal topography are genetically dissociable and furthermore that topographic mapping does not require proper sorting within the optic tract. These genetic results complement previous embryological experiments showing that regenerating axons can terminate topographically despite taking aberrant paths (Fujisawa, 1981) and that normal optic tract sorting is not sufficient for topographic targeting (Chien et al., 1995).

dak and *box* Encode Exostosin Family Members

To address the molecular mechanisms of optic tract sorting, we cloned the genes mutated in *dak* and *box*. *dak* was localized to LG7 using bulk segregant analysis, then fine mapped using a panel of >700 mutant F2 larvae from a WIK/Tübingen mapcross, using microsatellite markers and EST-derived SNPs to narrow the *dak* critical interval to 0.48 cM. We built a BAC/PAC contig across this interval and by partially sequencing one of the PACs identified *ext2* as a candidate gene for *dak*. We then sequenced the *ext2* coding sequences from three *dak* alleles and identified stop codons for each (Figure 3B; see Experimental Procedures). Given that these alleles encode early truncations and give similar phenotypes (van Eeden et al., 1996), they are all likely to be null.

box was localized to LG20 using genome scanning by hybridization to a SNP microarray chip (Stickney et al., 2002). Nearby SSLP markers (z5335 and fj59e01, 0.54 cM and 0.76 cM away from *box*, respectively) were mapped on a meiotic panel of 460 mutant embryos. At this point, the identification of *dak* as *ext2* and the similarity of the *box* and *dak* phenotypes suggested that *box* might be another EXT family member. We identified an *extl3* clone from EST sequences, and radiation hybrid mapping placed it very close to *box*. zEXTL3-CA1, a dinucleotide repeat marker within an *extl3* intron, showed very tight linkage to *box* (no recombinations in 920 meioses) (Figure 3A).

Sequencing of *extl3* from two *box* alleles revealed a nonsense mutation in the *tw24* allele and a missense mutation in *tm70g* (Figure 3B). The nonsense mutation (Gln to stop, AA 94) in *tw24* is an early truncation, before the glycosyltransferases domains, and is therefore very likely to create a null allele. The missense mutation (Asp to Asn, AA831) in *tm70g* likely creates a strong hypomorph or a null. This Asp residue is absolutely conserved in all known vertebrate and invertebrate EXT genes (Figure 3C). A recently derived crystal structure for Extl2 suggests that this Asp is located in the substrate binding site and is critical for activity (Pedersen et al., 2003). Biochemical analysis confirms that *tm70g* is strongly hypomorphic (see below). These molecular lesions indicate that the *box* phenotype is caused by loss of *extl3* function, consistent with the similar phenotypes of all eight known *box* alleles (van Eeden et al., 1996; Trowe et al., 1996).

Phylogenetic analysis shows that Dak/Ext2 and Box/Extl3 clearly cluster with Ext2 and Extl3 proteins from other species (Figure 3D) and are thus the true zebrafish orthologs of *ext2* and *extl3*, respectively.

HS Synthesis Is Disrupted in *dak* and *box*

Previous in vitro biochemical studies have shown that Ext2 is required for HS biosynthesis (Senay et al., 2000; McCormick et al., 2000) and have implicated Extl3 in an essential HS biosynthetic step (Kim et al., 2001, 2002) (Figure 3E). To determine directly if *ext2*/*dak* and *extl3*/*box* are required for HS synthesis in vivo, we analyzed HS levels in dak^{to273b} and box^{tm70g} mutants using disaccharide profiling (Toyoda et al., 2000). Glycosaminoglycans were partially purified from pooled mutants or siblings at 5 dpf, digested with a mixture of heparin lyases to generate disaccharide units, and separated on a reverse phase-ion pair HPLC column followed by fluorescent labeling. This method allows quantitative measurement of six structurally distinct disaccharide units: unsulfated uronic acid (ΔUA)-N-acetylglucosamine (GlcNAc); two different monosulfated units, ΔUA-GlcNS and ΔUA-GlcNAc6S; two disulfated units, ΔUA-GlcNS6S and ΔUA2S-GlcNS; and one trisulfated unit, ΔUA2S-GlcNS6S (Figure 4A and 4B). All species of disaccharides analyzed were drastically reduced in *dak* and *box*, with *dak* more severely affected than *box* (89% versus 78% reduction in total HS) (Figures 4A and 4B; Table 1). These data show that *dak*/*ext2* and *box*/*extl3* are each required for HS production and strongly suggest that the phenotypes of *dak* and *box* result from disruption of HS synthesis. Furthermore, they provide biochemical evidence that the *to273b* and *tm70g* alleles are indeed strong hypomorphs or nulls.

To test whether HS levels were reduced at earlier stages, we used the anti-HS antibody 10E4 (David et al., 1992) to stain heterozygous *dak* and *box* incrosses. By 24 hpf, staining was strongly reduced, though not eliminated, in *dak* and *box* mutants compared to their siblings (Figure 4C and data not shown). Thus, reduction of HS levels in mutants starts before RGC axons exit

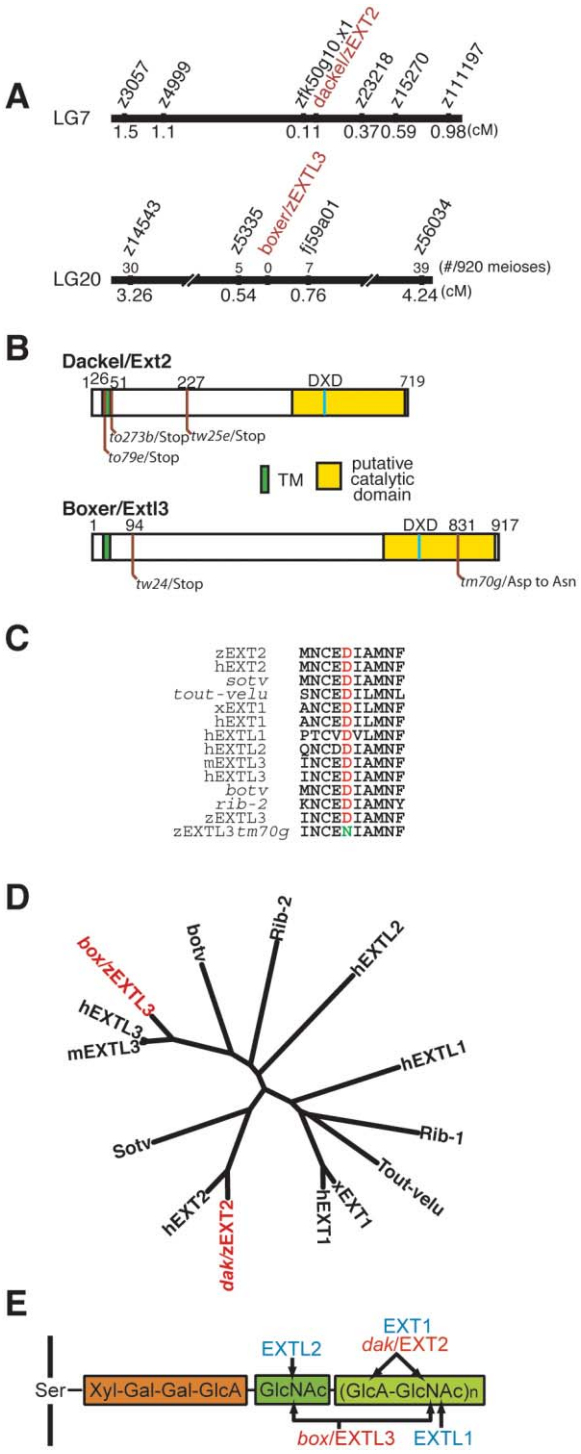

Figure 3. Molecular Cloning of *dak* and *box*

(A) Genetic maps of *dak* (upper) and *box* (lower). Number of recombinants in 920 meioses shown above the bar for *box* (not calculated for *dak* due to shared alleles). Numbers below the bars show genetic distances from each mutant.

(B) Predicted protein structures of *dak*/Ext2 (upper) and *box*/Extl3 (lower). Green box, transmembrane domains; yellow bars, putative N-acetylglucosaminyltransferase domains, showing the conserved DXD motif found in all glycosyltransferases. Red lines and numbers indicate positions of amino acid changes found in mutant alleles.

(C) Partial amino acid alignment shows that the Asp mutated in *box*^{tm70g} is absolutely conserved in all known exostosins. h, human; m, mouse; x, *Xenopus*; z, zebrafish. Ttv, Sotv, and Botv are *Drosophila* homologs of Ext1, Ext2, and Extl3, while Rib-1 and Rib-2 are *C. elegans* homologs of Ext1 and Extl3.

(D) Phylogenetic tree of known exostosins (CLUSTALW).

(E) Known biochemical functions of exostosin family members in the synthesis of heparan sulfate. A tetrasaccharide common to HSPGs and CSPGs (orange box) is attached to a serine residue in the core protein. The HS side chain is initiated by adding GlcNAc and extended by adding GlcA-GlcNAc disaccharide units, through distinct activities of different Ext enzymes.

the retina at ~32 hpf. To characterize HS distribution at the time of retinal axon outgrowth, we double stained 50 hpf wild-types with 10E4 and znp-1, an antibody that marks growing retinal axons as well as other forebrain axons. As seen in the visual systems of other animals (Halfter, 1993; Chung et al., 2001), HS is widely distributed throughout the brain: colocalized with the retinal axons, on the surfaces of neuroepithelial cells, and at high levels in basal laminae (Figures 4D–4G). This distribution is consistent with either growth cone-autonomous or nonautonomous roles for HSPGs in optic tract sorting.

Both *ext2* and *extl3* Are Maternally Provided and Broadly Expressed throughout Embryogenesis

The phenotypes of *dak* and *box* suggest that these genes should be expressed in the developing jaw, fin buds, and eyes or optic tract. Whole-mount in situ hybridization analysis showed that both *ext2* and *extl3* are highly expressed at the four-cell stage, indicating that they are maternally supplied (Figures 5A and 5D). At 50% epiboly through the ten-somite stage, *ext2* and *extl3* are ubiquitously expressed throughout the embryo, with distinct expression in somites (Figures 5B, 5E, and 5F). At 24 and 36 hpf, their expression becomes restricted to the nervous system but remains broad therein (Figures 5C and 5G). Both genes are clearly expressed in the pectoral fins at 36 hpf and 48 hpf (arrows in Figures 5C and 5H). At later stages, *ext2* and *extl3* expression patterns remain broad, with expression levels weakening by 72 hpf (data not shown). Both transcripts are faintly expressed in the retina at 24 and 36 hpf and are strongly expressed in the brain at these stages.

In vertebrates, both Ext1 and Ext2 are thought to be absolutely required for HS synthesis (Lin et al., 2000; McCormick et al., 2000). The requirement for Ext2 is supported by our disaccharide profiling of *dak* (Figure 4A). The in vivo function of *extl3* has been less clear. By carrying out HPLC analysis of *box* (*extl3*) mutants, we found that Extl3 is required for most, if not all, HS synthesis (Figure 4B). While expression in the brain, eye, pectoral fins, and developing branchial arches is consistent with the *dak* and *box* phenotypes, it is quite striking that both mutants have specific phenotypes despite the broad expression of both genes. HS is required in many developmental processes, and indeed a knockout mouse lacking Ext1 dies during gastrulation (Lin et al., 2000). Why then do *dak* and *box* embryos lack early phenotypes? We believe that this is due to maternally supplied *ext2* and *extl3* function, which allows homozy-

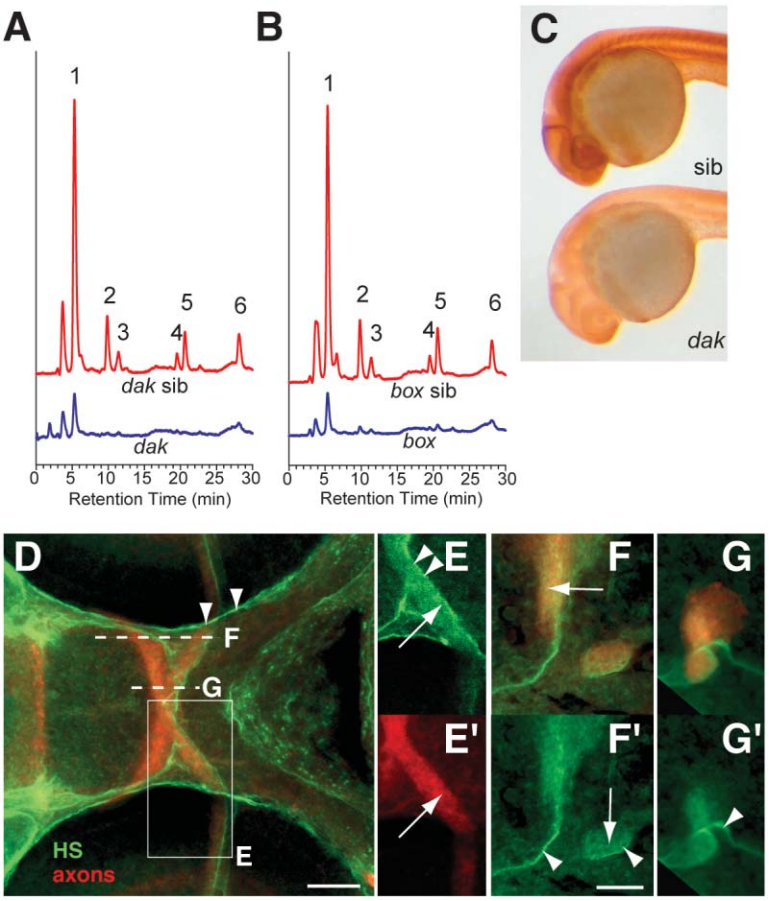

Figure 4. Heparan Sulfate Is Widely Distributed in Wild-Type Brains and Drastically Reduced in *dak* and *box*

(A and B) HS disaccharide profiles of *dak*^{to273b} and *box*^{tm70g} mutants (blue) and their sibs (red) at 5 dpf analyzed by HPLC. All disaccharide units were drastically reduced in mutants, with *dak* more affected than *box*. 1, unsulfated $\Delta^{4,5}$-unsaturated hexuronate-N-acetyl glucosamine (ΔUA-GlcNAc); 2, ΔUA-N-sulfated glucosamine (ΔUA-GlcNS); 3, ΔUA-6-O-sulfated GlcNAc (ΔUA-GlcNAc6S); 4, ΔUA-N-sulfated, 6-O-sulfated glucosamine (ΔUA-GlcNS6S); 5, 2-O-sulfated ΔUA-N-sulfated glucosamine (ΔUA2S-GlcNS); 6, 2-O-sulfated ΔUA-N-sulfated, 6-O-sulfated glucosamine (ΔUA2S-GlcNS6S).

(C) Staining with 10E4 antibody shows that HS is significantly reduced in *dak* embryos relative to wt siblings at 24 hpf.

(D–G) Double labeling of 50 hpf WT embryo with 10E4 (green) and znp-1 (red). Rostral is to the left. (D) Confocal projection, ventral view, showing strong HS staining in basal lamina (arrowheads). Box and dashed lines show locations of the single confocal sections shown in (E)–(G). (E and E′) Single section, ventral view with channels separated, showing HS staining in the optic nerve (arrows) and basal lamina (arrowheads). (F, F′, G, and G′) Single sagittal sections, showing merged channels (F and G) and HS staining only (F′ and G′). There is strong HS staining in basal lamina (arrowheads) and clear HS staining in the optic nerve and optic tract (arrows).

gote mutants to escape an early requirement for *dak* and *box* function, revealing their required functions later in development. We presume that most or all of the remaining HS at 5 dpf (Figure 4) is due to maternal function. Consistent with this hypothesis, injection of a translation-blocking antisense morpholino against *ext2*, which should knock down both maternal and zygotic function, leads to severely compromised gastrulation (H.R., unpublished data).

box Phenotypes Can Be Rescued by *extl3* mRNA

If *extl3* is indeed the gene disrupted in *box*, we reasoned that it might be possible to rescue *box* phenotypes by injecting one-cell embryos with wt *extl3* mRNA, which would be inherited by all cells in the embryo, mimicking the normal broad expression of *extl3*. Injections were done blind to genotype, and mutants were identified retrospectively by PCR genotyping. Overexpression of *extl3* was able to rescue the tract sorting error almost completely (Figure 2B and Figure 6A). Another *box* phenotype, shortened pectoral fins (van Eeden et al., 1996), was also rescued by *extl3* overexpression (Figures 6B–6E), with rescued pectoral fins being significantly longer than those of uninjected mutants. Overexpression itself does not cause gross defects, since the pectoral fins and retinotectal development of wt embryos injected with wt *extl3* were normal (Figure 6E and data not shown). As a control, we injected mutant mRNA for the *box*^{tm70g} allele at the same dose used for wt mRNA and were unable to rescue the pectoral fin phenotype (data not shown), confirming that *box*^{tm70g} Extl3 protein has reduced function. The fact that *box* could be rescued by RNA injection is consistent with a permissive role for *extl3* during development.

Development of Brain and Axon Tracts Are Grossly Normal in *dak* and *box*

One possible explanation for optic tract missorting might be that brain patterning is defective in *dak* and *box*. Indeed, a conditional knockout of mouse *Ext1*

Table 1. Quantitation of HPLC Disaccharide Profiling of *dak* and *box*

	UA-GlcNAc	UA-GlcNS	UA-GlcNAc6S	UA-GlcNS6S	UA2S-GlcNS	UA2S-GlcNS6S	Total
dak	84.3 ± 1.3	100 ± 0	93.7 ± 6.3	100 ± 0	93.7 ± 6.3	85.0 ± 6.1	89.1 ± 1.7
box	76.8 ± 9.0	94.7 ± 5.3	80.4 ± 4.1	95.3 ± 4.7	70.5 ± 16.9	74.2 ± 4.7	78.3 ± 6.8

Percentage decreases of HS disaccharide content (ng/mg) in *dak* and *box* at 5 dpf are shown compared to sibs. Abbreviations as in Figure 4. Values are means ± 1/2 range of duplicate measurements.

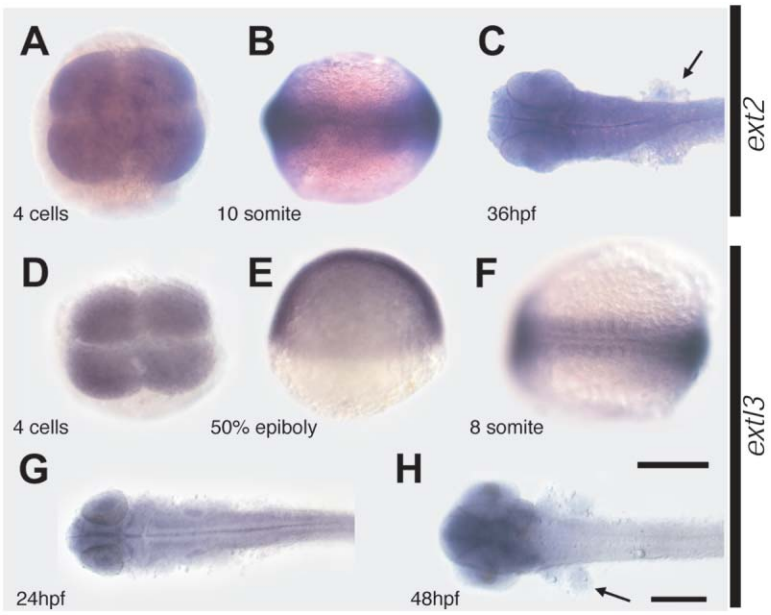

Figure 5. In Situ Hybridization for *ext2* and *extl3*

Both genes are maternally supplied and broadly expressed during embryogenesis, with expression restricted to the brain as development proceeds. (A–C) *ext2*; (D–H) *extl3*; (A and D) four-cell stage; (B) ten-somite stage; (C) 36 hpf; (E) 50% epiboly; (F) eight-somite stage; (G) 24 hpf; (H) 48 hpf; (C, G, and H) Dorsal views. Arrows in (C) and (H) indicate expression in pectoral fin buds. Scale bar, 200 μm.

shows strong defects in early brain patterning (*Nes-Ext1*; Inatani et al., 2003). To test this possibility, we examined the expression of *ptc1* and *fgf8*, markers for early brain patterning, and *isl1*, a marker for early neurogenesis (Inoue et al., 1994), in 24 hpf mutant embryos. No difference was detected between wild-type and mutants (Figures 7A–7L), suggesting that brain development is largely normal in *dak* and *box* at this stage.

Changes in brain patterning would be expected to disrupt the early axon scaffold, and indeed this occurs in *Nes-Ext1* mutants (Inatani et al., 2003). We therefore tested whether *dak* or *box* mutations affect the development of axon tracts by immunostaining embryos with anti-acetylated tubulin antibody at 24 hpf. Both *dak* and *box* were indistinguishable from wild-type at this stage, with apparently normal anterior and postoptic commissures as well as other forebrain tracts (Figures 7M–7P), again in contrast to *Nes-Ext1* mice.

Since hedgehog (HH) signaling is a key pathway whose disruption is responsible for phenotypes of the *Drosophila ttv*/ext1 mutant (Bellaiche et al., 1998), we wondered whether it plays a similar role in *dak* and *box*. The HH receptor *ptc1* is induced in response to HH signaling (Lewis et al., 1999). In contrast to *ttv*, we did not detect any changes of *ptc1* expression at 24 hpf or even 72 hpf (Figures 7A, 7B, 7G, and 7H; data not shown). *fgf8* is known to upregulate its own expression (Shanmugalingam et al., 2000), and its expression was also normal (Figures 7C, 7D, 7I, and 7J), in contrast to Nes-Ext1 mice (Inatani et al., 2003). Therefore, it appears that both HH and FGF8 signaling are largely unaffected during early brain patterning in *dak* and *box* embryos.

Removing Both *dak* and *box* Function Causes Strong Pathfinding Phenotypes

Biochemical studies of Ext2 and Extl3 suggest that these enzymes act in a linear pathway and are both required for HS synthesis (Duncan et al., 2001; Figure 3E). This is supported by drastic reductions in HS in *dak* or *box* mutants (Figures 4A–4C). Residual HS found in *dak* mutants is presumably due to maternal Ext2 acting together with maternal and zygotic Extl3, while residual HS in *box* would be due to maternal Extl3 acting with maternal and zygotic Ext2. This implies that in *box;dak* double mutants, HS should be reduced even further, since it can only be produced by maternal Ext2 acting with maternal Extl3.

Consistent with this prediction, we found retinotectal phenotypes in 5 dpf *box;dak* larvae that were stronger than those seen in either single mutant. Overall morphology of these mutant larvae (identified by PCR genotyping) was similar to single mutants, except for a slightly shorter body and mild defects in somite development. However, in addition to missorting phenotypes similar to those in single mutants, retinal axons in double mutants showed several *pathfinding* phenotypes in which axons left the optic tract. First, ipsilateral projections were formed by axons that left the optic tract shortly after the chiasm, then crossed the dorsal midline (Figures 8A, 8B, and 8E–8G). Such ipsilateral axons are seen rarely in wild-types at 5 dpf, are much more common in *dak* and *box* (wt, 1/9 embryos; *dak*, 7/10; *box*, 7/12), and were seen in almost all *box;dak* double mutants examined (17/19). Furthermore, many more axons took this ipsilateral route in *box;dak* compared with *box* or *dak* single mutants (Figure 8; data not shown). Interestingly, axons that reached either tectum still projected topographically in double mutants (Figures 8B, 8F, and 8G). Ipsilateral projections were also mildly enhanced in *box/+;dak/dak* and *box/box;dak/+* mutants (data not shown).

Other double mutant phenotypes were more dramatic (Figures 8C, 8F, and 8G), including anterior projections into the forebrain (1/19 double mutants), posterior projections into ventral hindbrain (5/19), and projections into the opposite eye (7/19). These errors are strikingly reminiscent of *astray* (*robo2*) mutants (Fricke et al., 2001; Hutson and Chien, 2002; Figures 8D and 8H). Indeed, of all known zebrafish mutants, *astray* is the only one

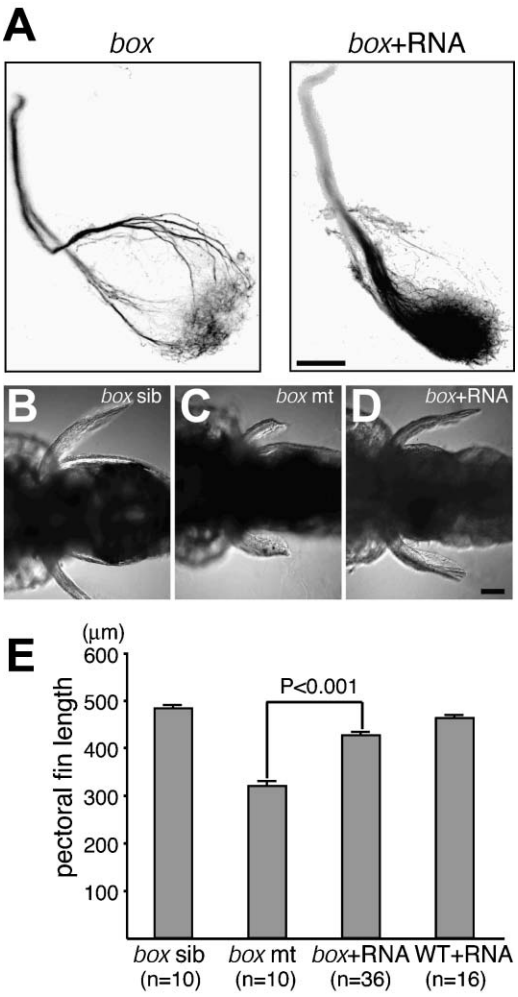

Figure 6. *extl3* mRNA Overexpression Rescues Optic Tract Sorting and Pectoral Fin Defects in *box*

(A) Inverted images of retinotectal projections of *box*^{tm70g} and rescued *box* mutants at 5 dpf. (Left) *box*; (right) *box* injected with *extl3* mRNA. Dorsonasal axon missorting is rescued by injecting *extl3* mRNA. See Figure 2B for quantitation.

(B–E) Rescue for pectoral fin defects. (B) wt pectoral fin. (C) *box* pectoral fin. (D) *box* pectoral fin after rescue. (E) Lengths of pectoral fins. The shortened pectoral fin of *box* is significantly rescued by injecting *extl3* mRNA. Scale bars, 50 μm in (A) and 100 μm in (D).

in which retinal axons project to the ventral hindbrain or into the opposite eye (Karlstrom et al., 1996; Trowe et al., 1996). Similar phenotypes were also seen after morpholino knockdown of *slit1a*, the only *slit* expressed in the optic tract (L.D. Hutson and C.-B.C., unpublished data). Together with studies in other systems that show that Slit-Robo signaling is potentiated by HSPGs (e.g., Hu, 2001; see Discussion for others), this suggests that the further reduction in HS levels in *box;dak* mutants causes these pathfinding phenotypes by compromising Slit-Robo signaling.

Might the missorting seen in *box* or *dak* single mutants also be due to defective Robo2 signaling? To address this directly, we analyzed homozygotes of *ast*^{ti272z}, a receptor null allele (Fricke et al., 2001). *ast* pathfinding phenotypes were similar to those seen in *box;dak*, except that tract sorting was unaffected. Those dorsal axons that stayed in the optic tract were sorted normally in the ventral brachium (Figures 8D and 8H). In order to quantitate sorting, we chose *ast* mutants in which the overall shape of the optic tract was intact (9/40), so that we could reliably measure MIs, and found that sorting was nearly as good as wild-type (MI 2.8%; Figure 2B; Figures 8D and 8H). As a further test, we generated *box*^{tm70g}/*box*^{tm70g}; *ast*^{ti272z} /+ larvae. Removing one copy of *robo2* in an *extl3* mutant background did not yield a significant increase in missorting compared to *box* single mutants ($p = 0.11$; Figure 2B). These data show that Robo2 does not play a major role in optic tract sorting.

Discussion

Sorting of retinal axons in the optic tract was described in adult cichlids by Scholes (1979), but nothing has been known of the underlying developmental mechanisms. We find here that the zebrafish optic tract is sorted early in retinotectal development (by 60 hpf), with a few errant axons that disappear by 5 dpf. Mutations in the glycosyltransferases *ext2* and *extl3* are responsible for the phenotypes of *dak* and *box*, implicating HSPG function in optic tract sorting.

ext2 and *extl3* Are Required for HS Synthesis

Drosophila mutants in *ext2* (*sotv*) and *extl3* (*botv*) have recently been isolated (Bornemann et al., 2004; Han et al., 2004; Takei et al., 2004), but no vertebrate mutants have been available. *dak* and *box* are thus useful tools to study the roles of these glycosyltransferases in vivo. In vitro biochemical studies show that Ext2 possesses GlcNAc and GlcA transferase activity and acts together with Ext1 to extend the HS chain by polymerizing the disaccharide repeats of HSPGs (Lind et al., 1998; McCormick et al., 2000). Our HPLC data for *dak* clearly demonstrate that vertebrate Ext2 is necessary for all or nearly all HS synthesis in vivo. Extl3 has GlcNAc transferase I and II activities (Kim et al., 2001) and thus is generally thought to act in initiation or extension of the HS chain (Figure 3E). An alternate hypothesis, that Extl3 acts to *terminate* HS chains, has been suggested based on experiments in which Ext1/Ext2 copolymerase could add HS chains in the absence of Extl3 (Busse and Kusche-Gullberg, 2003; Kim et al., 2003). Our *box* HPLC data argue that termination is not a major function for Extl3 in vivo; rather, Extl3 is necessary for most or all HS synthesis.

Both by HPLC and by immunostaining, residual HS levels are lower in *dak* than in *box* (Figure 4; Table 1; data not shown), correlating with the stronger pectoral fin phenotype and earlier tract sorting phenotype (Figure 2) of *dak*. There are two possible explanations. First, maternal function may persist longer for *box* than for *dak*, because of differences in protein levels or stability. Second, Extl1 and Extl2 may together partially substitute for Extl3, since they have overlapping enzymatic activities (Figure 3E). In contrast, Ext2 is thought to be absolutely required for HS extension (McCormick et al., 2000).

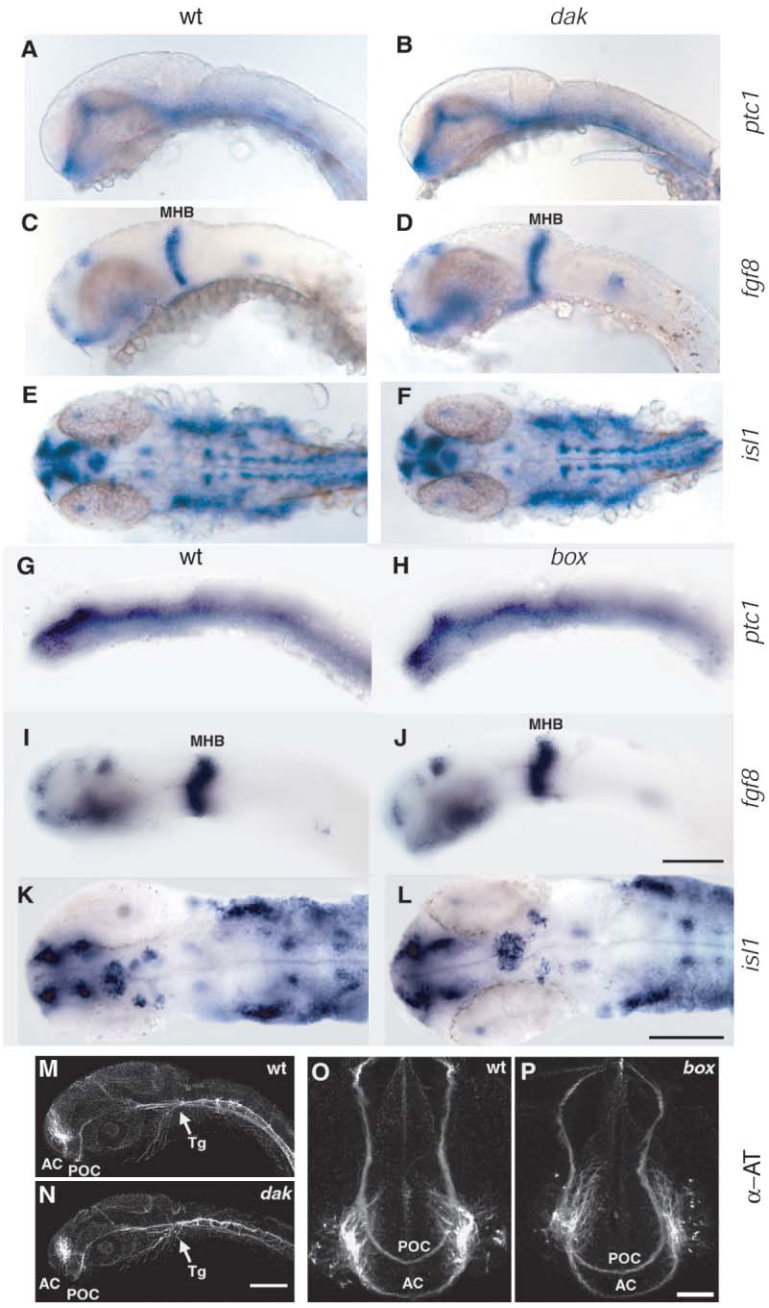

Figure 7. Development of the Brain and Early Axon Tracts Are Grossly Normal in *dak* and *box*

(A, C, E, G, I, K, M, and O) Wild-type siblings. (B, D, F, and N) *dak*. (H, J, L, and P) *box*. (A)–(F), (O), and (P) at 28 hpf; (G)–(N) at 24 hpf. Expression of *ptc1* (A, B, G, and H), *fgf8* (C, D, I, and J), and *isl1* (E, F, K, and L) was examined by whole-mount in situ hybridization. Axon tracts were visualized with anti-acetylated tubulin (M–P). Eyes removed in (G) and (H). (A–D and G–J) Lateral views. (E, F, and K–N) Dorsal views. (O and P) Anterior views. Scale bars, 100 μm (A–N) and 50 μm (O and P). AC, anterior commissure; MHB, midbrain-hindbrain boundary; POC, posterior commissure; Tg, trigeminal ganglion; α-AT, anti-acetylated tubulin staining.

Early Brain Patterning Is Unaffected by Loss of Zygotic *ext2* or *extl3*

HSPGs are critical cofactors for several developmental signaling pathways. Hh, Wnt, and Bmp signaling are all disrupted in *Drosophila* mutants with defective HS synthesis, including *ttv*, *sotv*, and *botv* (Bellaiche et al., 1998; The et al., 1999; Bornemann et al., 2004; Han et al., 2004; Takei et al., 2004). Mouse embryos lacking *Ext1* function do not gastrulate (Lin et al., 2000). Conditional inactivation of *Ext1* using a nestin-Cre driver line removes *Ext1* function only after E9.5, thus overcoming this early requirement. These *Nes-Ext1* null embryos show brain patterning defects that correlate with changes in Fgf signaling, as well as defects in midline guidance by forebrain commissural axons and retinal axons (Inatani et al., 2003).

The lack of zygotic HSPG synthesis enzymes in *dak* and *box* should eventually also compromise multiple signaling pathways. However, the phenotypes of *dak* and *box* are much more subtle than that of *Nes-Ext1* null mice. At 24–28 hpf, the initial patterning of the forebrain, midbrain-hindbrain boundary, and initial axon scaffold are all apparently normal, and neither *dak* nor *box* shows changes in expression of *ptc1* and *fgf8* (Figure 7), reporters of Hh and Fgf signaling (Lewis et al., 1999; Shanmugalingam et al., 2000). Thus, gross mispatterning of the optic tract is unlikely to cause the retinal axon sorting errors, although we cannot rule out subtle patterning

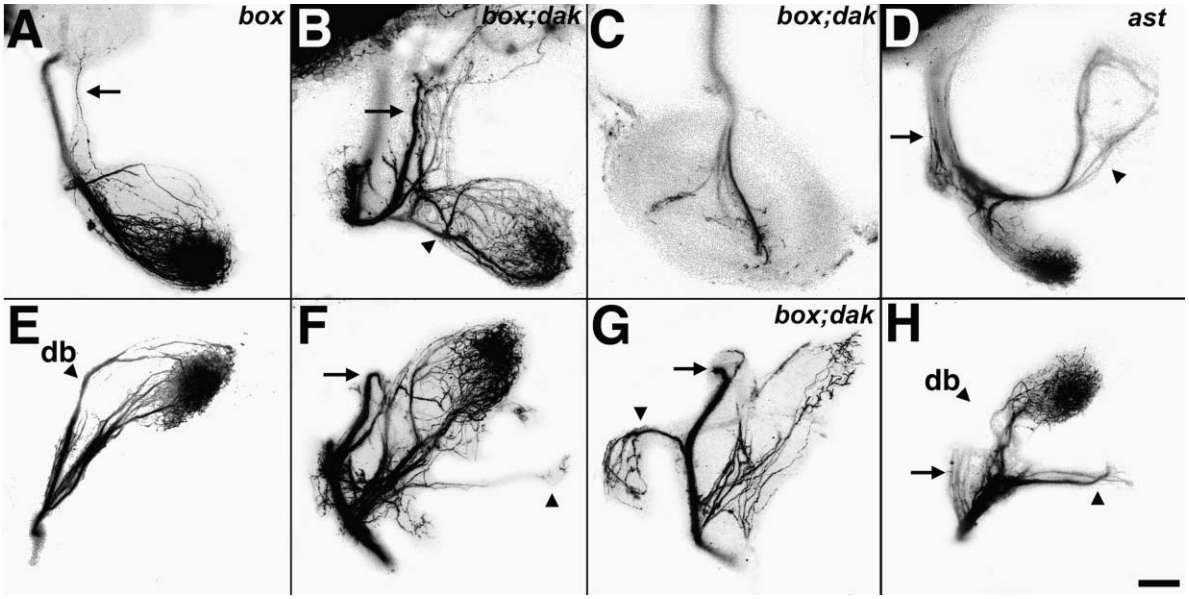

Figure 8. Removing Both *dak* and *box* Function Enhances Ipsilateral Projections and Leads to Pathfinding Errors that Phenocopy *ast*

(A and E) A *box*^{tm70g} mutant shown in dorsal and lateral views. Many axons missort through the dorsal brachium (db in [E]), while a few axons recross the dorsal midline to the ipsilateral tectum (arrow in [A]). (B, C, F, and G) Three *box*^{tm70g}*;dak*^{to273b} double mutants. The first shows strong ipsilateral projections (arrows in [B] and [F]) and a posterior projection (arrowhead in [F]). The second has an interretinal projection (C). The third has a strong ipsilateral projection (arrow in [G]) and an anterior projection (arrowhead in [G]). (D and H) An *ast*^{ti272z} mutant shown in dorsal and lateral views. Some axons leave the optic tract early and project across the dorsal midline (arrows); others project posteriorly to ventral hindbrain (arrowheads). None missort in the dorsal brachium (db). All mutants were labeled dorsonasally. Scale bar, 50 μm.

defects. The fact that tract sorting is nearly normal in *box* at 3 dpf, only going awry by 5 dpf, further argues that initial brain patterning is normal in *box*.

Is HS synthesis unnecessary for patterning the zebrafish brain? This seems unlikely. Instead, we believe that maternal *ext2* and *extl3* function supplies HSPGs to carry the embryo through early development. Indeed, removing maternal *ext2* function using a translation-blocking morpholino disrupts gastrulation (H.R., unpublished data). Furthermore, morpholino knockdown of the HS-modifying enzyme 6-O-sulfotransferase (6-OST) results in disrupted expression of *shh* in the brain at 24 hpf (Bink et al., 2003), suggesting that HS is required during brain patterning. In *box* or *dak* zygotic mutants, the speed of zebrafish development means that HSPGs do not become limiting until after initial brain pattern is established, which makes it possible to study later functions that require HSPGs. If not for maternal function, mutants for HS synthesis would not have been recovered in the retinotectal screen.

Roles of HSPGs in Axon Guidance and Sorting

Several embryological studies have shown that proteoglycans including HSPGs play important roles in axon guidance in different contexts (reviewed in Bandtlow and Zimmermann, 2000; Lee and Chien, 2004). In *Xenopus*, either adding exogenous HS or removing HS with heparitinase causes retinal axons to bypass the tectum (Walz et al., 1997). This bypass depends on specific HS sulfation forms (Irie et al., 2002). Some bypassing axons project along the ventral border of the tectum, while others project along the anterior border of the tectum and cross the dorsal midline. These latter projections are intriguingly similar to the ipsilateral projections seen in *ast*, *box*, *dak*, and especially *box;dak* double mutants (Figure 8). In the newborn hamster, the dorsal tectal midline inhibits the aberrant crossing of retinal axons; this inhibition has been attributed to unidentified HSPGs and CSPGs expressed in this region (Hoffman-Kim et al., 1998). Thus, it seems that the dorsal midline may form a barrier to retinal axons, whose inhibitory character depends on HSPG and perhaps Slit-Robo function. The enhanced ipsilateral projections in *box;dak* double mutants may be due to further reductions in HS levels.

Apart from the ipsilateral projections, the retinal projection in HS-manipulated *Xenopus* is quite different from *box* and *dak* mutants. This may result either from differences in overall HS levels or from differences in particular forms of HS. It would be especially interesting to repeat the *Xenopus* experiments and assay optic tract sorting.

Manipulations of Fgf signaling in *Xenopus* retinal axons give projection defects similar to HSPG manipulations (McFarlane et al., 1995, 1996), consistent with the known role of HSPGs as essential cofactors for Fgf-Fgfr signaling (Schlessinger et al., 1995). Three reasons suggest that the tract sorting defect in *dak* and *box* is not due to altered Fgf signaling. First, *fgf8* expression appears unaffected in both mutants. Second, retinal axons in *dak* and *box* enter the tectum without difficulty, in contrast to the tectal bypass phenotype seen after manipulating HS or Fgf signaling in *Xenopus* (McFarlane et al., 1995, 1996; Walz et al., 1997), or after pharmacological inhibition of Fgf signaling in zebrafish (Masai et al., 2003). Third, the retinotectal phenotypes of the zebrafish *ace* (*fgf8*) mutant are much more severe than

those of *dak* and *box*. In *ace*, retinal axons overshoot the tectum, show topographic errors on the tectum, and have retinal polarity defects (Picker et al., 1999). Possibly as a result of these polarity defects, both dorsal and ventral retinal axons missort in the optic tract of *ace* mutants.

Interactions with Slit/Robo Signaling

Three sets of recent genetic experiments have shown roles for HSPGs in axon guidance; in all three, HSPGs appear to interact with Slit/Robo signaling. First, *Drosophila* mutants for the cell surface HSPG syndecan affect midline axon guidance, interact genetically with *slit* and *robo*, and disrupt the extracellular distribution of Slit (Steigemann et al., 2004; Johnson et al., 2004). Second, genes that control sulfation and epimerization of HS are required for axon guidance in *C. elegans* and interact with Slit and Robo genes (Bülow and Hobert, 2004). Third, while retinal axons in *Nes-Ext1*$^{null/+}$ heterozygotes and *Slit2*$^{-/-}$ homozygotes project largely normally, *Nes-Ext1*$^{null/+}$; *Slit2*$^{-/-}$ compound mutants show strong optic chiasm defects, primarily retinoretinal projections reminiscent of *box;dak* double mutants (Inatani et al., 2003). These in vivo results reinforce previous in vitro experiments showing that HS potentiates the inhibitory effect of Slit2 in neuronal migration and axon guidance (Hu, 2001) and biochemical experiments showing that Slits bind the HSPG glypican-1 (Liang et al., 1999; Ronca et al., 2001).

In zebrafish, *ast* (*robo2*) is the only *robo* gene expressed in RGCs as their axons pathfind (Fricke et al., 2001; Lee et al., 2001). *ast* null mutants show normal tract sorting, implying that *robo2* is not required for this process. In *box* and *dak* single mutants, HS levels are significantly reduced, but retinal projection defects are quite distinct from *ast*, except for the ipsilateral projections across the dorsal midline that are seen in all three mutants. However, when we further reduced HS levels by generating *box;dak* double mutants, retinal axons left the optic tract, projecting anteriorly, posteriorly, and into the other eye—a set of errors characteristic of *ast* mutants. This is consistent with the hypothesis that Robo2 signaling requires a low minimal level of HS. Based on comparison of the single and double *box* and *dak* phenotypes, we propose a model in which there are two critical thresholds for HS levels, one higher and one lower. In single mutants, HS levels drop below the higher threshold, which is required for optic tract sorting through a Slit-Robo-independent mechanism. In double mutants, HS levels drop below the lower threshold, which is required for Slit-Robo signaling.

Other Developmental Roles of HSPGs

In addition to optic tract sorting errors, *dak* and *box* also display defects in pectoral fin and jaw formation, demonstrating that HSPGs are required for both processes. In the pectoral fin, the homolog of the tetrapod forelimb (Grandel and Schulte-Merker, 1998), the requirement for HSPGs is consistent with known mechanisms for limb patterning. Fgfs, Shh, and Wnts are essential for limb formation (Capdevila and Izpisua Belmonte, 2001), and their signaling pathways are all potentiated by HSPGs (Nybakken and Perrimon, 2002; Princivalle and de Agostini, 2002). Indeed, in *dak* embryos, expression of *shh* in the fin bud is initially normal but fails to be maintained (Grandel et al., 2000). Further analysis of *dak* and *box* should shed light on the roles of HSPGs in fin and jaw formation. It would also be of interest to conditionally inactivate mouse *Ext1* in the limb buds or branchial arches.

What Is the Role of HSPGs in Optic Tract Sorting?

Optic tract sorting begins early and takes place shortly after midline crossing. However, interactions with the midline are not required, since tract sorting is normal in mutants in which retinal axons fail to cross the midline (Trowe et al., 1996; Karlstrom et al., 1996). The *dak* phenotype is evident from 60 hpf onward, while missorting in *box* seems to occur only after 72 hpf. Thus, zygotic *dak* function is required for sorting of both early and late axons, while zygotic *box* function is only required for later axons (new axons are added continually during this period). The fact that *box* mutants have nearly normal sorting at 72 hpf, but clear missorting at 5 dpf, suggests that correct sorting of early axons is not sufficient for sorting later axons.

What then is the mechanism of optic tract sorting? There must be underlying molecular differences between dorsal and ventral axons, since they show distinct behaviors in wild-type, and only dorsal axons missort in *dak* and *box*. The simplest model is that (1) tract sorting requires a guidance receptor specifically active in dorsal axons, and (2) the ligand for this receptor is expressed asymmetrically, either in the diencephalon or on the retinal axons themselves, so that either the dorsal brachium is repulsive for axons from dorsal retina, or the ventral brachium is attractive.

Assuming that the missorting seen in *box* and *dak* is indeed not due to some subtle brain mispatterning, there are three possibilities for how HSPGs might act in this model. First, an HSPG could be a required cofactor in the process. Second, the receptor expressed on dorsal axons could be a cell surface HSPG such as a syndecan or a glypican. Third, the cognate ligand could be an HSPG—either a cell surface HSPG or an ECM HSPG such as perlecan or agrin. Distinguishing between these possibilities will require testing of the appropriate candidate core proteins.

Three other known mutants also have tract sorting errors. *pinscher* (*pic*) has fin and especially jaw phenotypes reminiscent of *dak* and *box*, with which it forms a phenotypic class (Trowe et al., 1996). Two other mutants from the Tübingen screen, *nevermind* (*nev*) and *whocares* (*woe*), form another class. *nev* and *woe* have normal fins and jaws, show optic tract sorting defects by dorsonasal axons, and also show topographic targeting errors on the tectum (Trowe et al., 1996; A. Pittman and C.-B.C., unpublished data). Cloning and analysis of these three mutants may help to further elucidate the molecular pathways controlling optic tract sorting.

Experimental Procedures

Visualization of Optic Tract Sorting

Embryos at 5 dpf were fixed with 4% PFA overnight, and RGCs in the dorsonasal and ventrotemporal quadrants of their retinae were anterogradely labeled with the lipophilic dyes DiI and DiO using a vibrating needle injector (Baier et al., 1996). Occasionally, DiI alone

was injected to visualize dorsonasal axons specifically. All retinotectal projections are shown as projected confocal Z series (Olympus Fluoview 300; 5 μm z spacing). MIs were calculated (see Figure 2A for an example) using ImageJ (W.S. Rasband, National Institutes of Health, http://rsb.info.nih.gov/ij/, 1997–2003). PMT voltage and gain were held constant throughout the Z series. A reference line was drawn parallel to the mediolateral axis, ~30% of the way from the chiasm to the posterior end of the tectum (Figure 3A). After reslicing the z stack along this line, a threshold was set between 25 and 35 out of a grayscale range of 0–255, areas were measured using the "Analyze Particles" option, and the MI was calculated as a ratio of areas: (dorsal brachium)/(dorsal and ventral brachia). Statistical comparisons of MIs used two-tailed Student's t tests.

Identification of *dak* and *box* Mutants

In addition to retinotectal projection defects that are visualized by dye injection, *dak* and *box* have completely penetrant pectoral fin and jaw phenotypes and lack swim bladders, allowing us to identify mutants after 3 dpf.

To identify younger homozygotes and double mutants, we genotyped embryos by designing cleaved amplified polymorphic sequence (CAPS) and derived CAPS (dCAPS) primers against the point mutations in *box*^{tm70g} and *dak*^{to273}, respectively (Neff et al., 2002) (*box*^{tm70g} CAPS primers, 5′-CATTCAGCCCTTGTCATGATT-3′ and 5′-CAGGATCACCAAGAATGACC-3′; *dak*^{to273} dCAPS primers, 5′-TGGA CAGGCTCATCATGTGT-3′ and 5′-CGGTCCAGACTCCATTCGGCTG AAGACTT-3′]. PCR conditions were 94°C, 2 min; 40 cycles of 94°C 1 min, 53°C 1 min, and 72°C 1 min; 72°C 10 min. Wild-type but not mutant PCR amplicons amplified with the *box* CAPS primers and *dak* dCAPS primers were digested by EcoRV and MseI, respectively, giving rise to 164 bp and 210 bp fragments for *box* and 163 bp and 30 bp fragments for *dak*, which were separated on 2% agarose and 3% Metaphor gels, respectively.

Cloning of *dak* and *box* Mutations

dak was rough mapped to LG7 using bulk segregant analysis (Geisler, 2002; http://wwwmap.tuebingen.mpg.de/) and fine mapped using microsatellite markers on >700 mutant larvae (for primer sequences and genetic map, see http://zebrafish.mgh.harvard.edu/zebrafish/index.htm). *dak* was mapped with high confidence to a 2 cM interval flanked by two markers, z4999 and z23218. Based upon the local radiation hybrid map, we designed primer pairs and identified SNPs against nearby ESTs (http://134.174.23.167/zonrh-mapper/RHLg/lg7.htm). One EST, fk50g10.x1, mapped 0.11 cM from *dak*, narrowing the *dak* interval to 0.48 cM. Using EST primer pairs to screen pooled PAC and BAC DNA, we assembled a partial PAC/BAC contig, then used a PAC/BAC end walk to assemble four clones that spanned the *dak* interval. One PAC, BZ2B14, was chosen for 2× shotgun sequencing; BLAST analysis identified the *ext2* genomic sequence.

A genome scan for *box* was performed using genomic DNA from 24 mutant embryos and 24 wild-type siblings, which were pooled and amplified by multiplex PCR for identified SNPs. Amplicons were hybridized to oligonucleotide microarrays as described (Stickney et al., 2002), identifying three linked SNPs on LG20 (ZSNP1549, ZSNP1590, ZSNP1591). Conventional SSLP markers were scored by standard methods (Talbot and Schier, 1999) to confirm and refine the map location of *box*. Rough mapping was carried out on 80 mutants, and then fine mapping was carried out on a panel of 460 mutants (920 meioses) using SSLP (z56034 and z14543) and SSCP/SNP markers (z5335 and fj59a01). An SSLP marker, zEXTL3-CA1, derived from an intronic CA repeat found in *extl3* genomic sequence (Sanger Institute) showed no recombinations away from *box* on our panel.

Allelic Sequencing

Initially, sequencing directly from cDNAs pooled from homozygous mutant larvae for three *dak* alleles, we could not identify any obvious mutations. However, we noticed reproducible base changes encoding for premature stop codons embedded underneath the wild-type trace for each allele: for *to79e*, TAC to TAA (aa 26/exon 1); for *to273b*, ATT GAG to ATA TAG (aa 50–51/exon1); for *tw25e*, TAT to TAA (aa 227/exon5). We presume that nonsense-mediated decay destabilizes mutant mRNAs, so that their sequences are obscured by wild-type maternal mRNA. Indeed, whole-mount in situ analysis demonstrates a strong reduction in *ext2* mRNA in 48hpf *dak* mutants (data not shown). We confirmed these mutations by sequencing exonic genomic PCR products.

Wild-type and mutant cDNA from *box*^{tm70g} was obtained by RT-PCR (Superscript II; Invitrogen) of RNA prepared from single embryos using Trizol (Invitrogen). For each embryo, genomic DNA was prepared simultaneously and genotyped using the SSLP marker for *extl3* (zEXTL3-CA1). For *box*^{tw24}, exons 1, 2, and 5 of *extl3* were amplified by genomic PCR from fixed wild-type and mutant embryos kindly provided by Silke Geiger-Rudolph (MPI Entwicklungsbiologie, Tübingen). The cDNA (*box*^{tm70g}) or genomic DNA (*box*^{tw24}) was sequenced on both strands to identify mismatches between wild-type and mutant. Mutations were confirmed in at least two independent embryos. The GenBank accession numbers for *ext2* and *extl3* are AY786508 and AY786436, respectively.

Rescue of *box* Phenotypes

The wt *extl3* coding sequence or mutant *extl3* harboring the *tm70g* point mutation was cloned into expression vector pCGE1 (L.D. Hutson, B. Mangum, and C.-B.C., unpublished data) using the Gateway system (Invitrogen), with or without a C-terminal GFP fusion, and used to synthesize sense mRNA by in vitro transcription (SP6 promoter; Ambion mMessage mMachine). *extl3* mRNA (500 pg) was injected into one-cell embryos from *box* heterozygote incrosses. Embryos were fixed at 5 dpf and genotyped using tail gDNA. Pectoral fin lengths were measured, and DiI was injected into dorsonasal retina to examine the retinotectal projection. Pectoral fin lengths were compared using unpaired two-tailed Student's t tests.

Preparation and HPLC Analysis of Heparan Sulfate Disaccharides

According to procedures adapted from those described in Toyoda et al. (2000), samples of 100 5 dpf zebrafish embryos were washed in distilled water, snap frozen, and lyophilized, then resuspended in 0.5 ml of 50 mM Tris/HCl [pH 8], 1 mM $CaCl_2$, 1% Triton X-100. They were sonicated two times for 30 s at 4–5 W before removal of a fraction for protein estimation (Pierce BCA Assay). Samples were then digested with 0.8 mg/ml protease for 16 hr at 55°C, heat inactivated at 96°C for 5 min, and incubated 2 hr at 37°C with 1 μl 1 M $MgCl_2$ and 0.5 μl (168.5 U) benzonase (Ledin et al., 2004). NaCl was added to 0.1 M, and insoluble material was removed by microcentrifugation for 10 min at 16,000 g. The solution was applied to an Ultrafree_MC DEAE membrane that had been equilibrated with sodium phosphate buffer (pH 6.0) containing 0.15 M NaCl. The fractions eluted with 1.0 M NaCl in the same buffer were collected, desalted both with Biomax-5 and by PD10 gel column filtration, lyophilized, and resuspended in 30 μl 0.03 M acetate buffer (pH 7.0) with 3.33 mM calcium acetate, 0.33 mIU heparinase, 0.33 mIU heparitinase II, and 0.33 mIU heparitinase I. The mixture was incubated at 37°C for 16 hr, lyophilized, and resuspended in 12 μl water to load onto the HPLC. HPLC conditions were as in Toyoda et al. (2000).

Double Mutant Analysis

Offspring of a *box*^{tm70g}/+ × *dak*^{to273}/+ cross were raised to adulthood. *box*/+; *dak*/+ double heterozygote carriers were identified by crossing and CAPS/dCAPS genotyping. Retinotectal projections of embryos from double heterozygote incrosses were visualized by injecting DiI into their dorsonasal retinae, and individual embryos were genotyped retrospectively for both genes using CAPS/dCAPS primers.

Whole-Mount In Situ Hybridization

Whole-mount in situ hybridization was performed as in Lee et al. (2001). Antisense probe for *ext2* used a full-length clone (fv22b10) linearized with SmaI and transcribed with SP6; that for *extl3* used a full-length clone of *extl3* linearized with NotI and transcribed with SP6. Negative controls with *extl3* sense probe showed only very weak background signals (data not shown). *ptc1*, *fgf8*, and *isl1* plasmids were kind gifts from the Yost, Grunwald, and Okamoto laboratories. After in situ hybridization, individual embryos were genotyped using tail gDNA, and images were taken using an Olympus Magnafire SP digital camera.

Whole-Mount Antibody Staining

Primary antibodies used were anti-HS (10E4; US Biological) at 1:50 and znp-1 (supernatant; developed by Bill Trevarrow and obtained from the Developmental Studies Hybridoma Bank) at 1:200. Secondary antibodies used were goat anti-IgM-HRP and goat anti-IgG2a-HRP (Southern Biotech) at 1:500. Embryos were fixed in 4% PFA, stored in MeOH, and permeabilized with proteinase K. 10E4 labeling of heterozygous incrosses at 24 and 48 hpf used DAB substrate (Sigma). For double labeling, embryos were stained sequentially using tyramide substrates (TSA-fluorescein and TSA-Cy3; Perkin Elmer), inactivating residual HRP after the first label using 0.1 N HCl for 10 min. Eyes were dissected away for lateral views, and embryos were mounted in Vectashield (Vector Labs).

Acknowledgments

We thank Silke Geiger-Rudolph for providing fixed *box* embryos; Louis Ross for technical support; and members of the Chien, Geisler, and Nüsslein-Volhard laboratories for advice and help. Thanks to Michael Granato for suggesting the use of dCAPS primers. We thank Christa Lanz, Günter Raddatz, and Stephan Schuster for shotgun sequencing the BZ2B14 PAC; and Gerg-Jörg Rauch and Axel Küchler for the initial mapping of *dak*. We also thank Maureen Condic for comments and discussion of the manuscript. This work was supported by a grant from the NSF (to C.-B.C.); by a Wellcome Trust grant (072346/Z/03/Z); by the Max Planck Society (to H.R.); and by NCI 5U01-CA91290 (to S.B.S). This work was also supported by a graduate fellowship from HHMI (to H.L.S.); NIH grant RR12349 (to W.S.T.); and by the DHGP (to R.G.).

Received: May 18, 2004
Revised: September 15, 2004
Accepted: November 1, 2004
Published: December 15, 2004

References

Baier, H., Klostermann, S., Trowe, T., Karlstrom, R.O., Nusslein-Volhard, C., and Bonhoeffer, F. (1996). Genetic dissection of the retinotectal projection. Development *123*, 415–425.

Bandtlow, C.E., and Zimmermann, D.R. (2000). Proteoglycans in the developing brain: new conceptual insights for old proteins. Physiol. Rev. *80*, 1267–1290.

Bellaiche, Y., The, I., and Perrimon, N. (1998). Tout-velu is a Drosophila homologue of the putative tumour suppressor EXT-1 and is needed for Hh diffusion. Nature *394*, 85–88.

Bink, R.J., Habuchi, H., Lele, Z., Dolk, E., Joore, J., Rauch, G.J., Geisler, R., Wilson, S.W., den Hertog, J., Kimata, K., and Zivkovic, D. (2003). Heparan sulfate 6-o-sulfotransferase is essential for muscle development in zebrafish. J. Biol. Chem. *278*, 31118–31127.

Bornemann, D.J., Duncan, J.E., Staatz, W., Selleck, S., and Warrior, R. (2004). Abrogation of heparan sulfate synthesis in Drosophila disrupts the Wingless, Hedgehog and Decapentaplegic signaling pathways. Development *131*, 1927–1938.

Bülow, H.E., and Hobert, O. (2004). Differential sulfations and epimerization define heparan sulfate specificity in nervous system development. Neuron *41*, 723–736.

Busse, M., and Kusche-Gullberg, M. (2003). In vitro polymerization of heparan sulfate backbone by the EXT proteins. J. Biol. Chem. *278*, 41333–41337.

Capdevila, J., and Izpisua Belmonte, J.C. (2001). Patterning mechanisms controlling vertebrate limb development. Annu. Rev. Cell Dev. Biol. *17*, 87–132.

Chan, S.O., and Guillery, R.W. (1994). Changes in fiber order in the optic nerve and tract of rat embryos. J. Comp. Neurol. *344*, 20–32.

Chien, C.-B., Cornel, E.M., and Holt, C.E. (1995). Absence of topography in precociously innervated tecta. Development *121*, 2621–2631.

Chung, K.Y., Leung, K.M., Lin, L., and Chan, S.O. (2001). Heparan sulfate proteoglycan expression in the optic chiasm of mouse embryos. J. Comp. Neurol. *436*, 236–247.

David, G., Bai, X.M., Van der Schueren, B., Cassiman, J.J., and Van den Berghe, H. (1992). Developmental changes in heparan sulfate expression: in situ detection with mAbs. J. Cell Biol. *119*, 961–975.

Duncan, G., McCormick, C., and Tufaro, F. (2001). The link between heparan sulfate and hereditary bone disease: finding a function for the EXT family of putative tumor suppressor proteins. J. Clin. Invest. *108*, 511–516.

Fricke, C., Lee, J.S., Geiger-Rudolph, S., Bonhoeffer, F., and Chien, C.B. (2001). astray, a zebrafish roundabout homolog required for retinal axon guidance. Science *292*, 507–510.

Fujisawa, H. (1981). Retinotopic analysis of fiber pathways in the regenerating retinotectal system of the adult newt cynops Pyrrhogaster. Brain Res. *206*, 27–37.

Geisler, R. (2002). Tübingen map of the zebrafish genome (http://wwwmap.tuebingen.mpg.de/).

Grandel, H., and Schulte-Merker, S. (1998). The development of the paired fins in the zebrafish (Danio rerio). Mech. Dev. *79*, 99–120.

Grandel, H., Draper, B.W., and Schulte-Merker, S. (2000). dackel acts in the ectoderm of the zebrafish pectoral fin bud to maintain AER signaling. Development *127*, 4169–4178.

Halfter, W. (1993). A heparan sulfate proteoglycan in developing avian axonal tracts. J. Neurosci. *13*, 2863–2873.

Han, C., Belenkaya, T.Y., Khodoun, M., Tauchi, M., and Lin, X. (2004). Distinct and collaborative roles of Drosophila EXT family proteins in morphogen signalling and gradient formation. Development *131*, 1563–1575.

Hoffman-Kim, D., Lander, A.D., and Jhaveri, S. (1998). Patterns of chondroitin sulfate immunoreactivity in the developing tectum reflect regional differences in glycosaminoglycan biosynthesis. J. Neurosci. *18*, 5881–5890.

Hu, H. (2001). Cell-surface heparan sulfate is involved in the repulsive guidance activities of Slit2 protein. Nat. Neurosci. *4*, 695–701.

Hutson, L.D., and Chien, C.B. (2002). Pathfinding and error correction by retinal axons: the role of astray/robo2. Neuron *33*, 205–217.

Inatani, M., Irie, F., Plump, A.S., Tessier-Lavigne, M., and Yamaguchi, Y. (2003). Mammalian brain morphogenesis and midline axon guidance require heparan sulfate. Science *302*, 1044–1046.

Inoue, A., Takahashi, M., Hatta, K., Hotta, Y., and Okamoto, H. (1994). Developmental regulation of islet-1 mRNA expression during neuronal differentiation in embryonic zebrafish. Dev. Dyn. *199*, 1–11.

Irie, A., Yates, E.A., Turnbull, J.E., and Holt, C.E. (2002). Specific heparan sulfate structures involved in retinal axon targeting. Development *129*, 61–70.

Johnson, K.G., Ghose, A., Epstein, E., Lincecum, J., O'Connor, M.B., and Van Vactor, D. (2004). Axonal heparan sulfate proteoglycans regulate the distribution and efficiency of the repellent Slit during midline axon guidance. Curr. Biol. *14*, 499–504.

Karlstrom, R.O., Trowe, T., Klostermann, S., Baier, H., Brand, M., Crawford, A.D., Grunewald, B., Haffter, P., Hoffmann, H., Meyer, S.U., et al. (1996). Zebrafish mutations affecting retinotectal axon pathfinding. Development *123*, 427–438.

Kim, B.T., Kitagawa, H., Tamura, J., Saito, T., Kusche-Gullberg, M., Lindahl, U., and Sugahara, K. (2001). Human tumor suppressor EXT gene family members EXTL1 and EXTL3 encode α1,4- N-acetylglucosaminyltransferases that likely are involved in heparan sulfate/heparin biosynthesis. Proc. Natl. Acad. Sci. USA *98*, 7176–7181.

Kim, B.T., Kitagawa, H., Tamura Ji, J., Kusche-Gullberg, M., Lindahl, U., and Sugahara, K. (2002). Demonstration of a novel gene DEXT3 of Drosophila melanogaster as the essential N-acetylglucosamine transferase in the heparan sulfate biosynthesis: chain initiation and elongation. J. Biol. Chem. *277*, 13659–13665.

Kim, B.T., Kitagawa, H., Tanaka, J., Tamura, J., and Sugahara, K. (2003). In vitro heparan sulfate polymerization: crucial roles of core protein moieties of primer substrates in addition to the EXT1-EXT2 interaction. J. Biol. Chem. *278*, 41618–41623.

Kitagawa, H., Egusa, N., Tamura, J.I., Kusche-Gullberg, M., Lindahl, U., and Sugahara, K. (2001). rib-2, a Caenorhabditis elegans homolog of the human tumor suppressor EXT genes encodes a novel α1,4-N-acetylglucosaminyltransferase involved in the biosynthetic initiation and elongation of heparan sulfate. J. Biol. Chem. *276*, 4834–4838.

Ledin, J., Staatz, W., Li, J.P., Gotte, M., Selleck, S., Kjellen, L., and Spillmann, D. (2004). Heparan sulfate structure in mice with genetically modified heparan sulfate production. J. Biol. Chem. *279*, 42732–42741.

Lee, J.S., and Chien, C.B. (2004). When sugars guide axons: new lessons from HSPG mutants. Nat. Rev. Genetics, in press.

Lee, J.S., Ray, R., and Chien, C.B. (2001). Cloning and expression of three zebrafish roundabout homologs suggest roles in axon guidance and cell migration. Dev. Dyn. *221*, 216–230.

Leung, K.M., Taylor, J.S., and Chan, S.O. (2003). Enzymatic removal of chondroitin sulphates abolishes the age-related axon order in the optic tract of mouse embryos. Eur. J. Neurosci. *17*, 1755–1767.

Lewis, K.E., Concordet, J.P., and Ingham, P.W. (1999). Characterisation of a second patched gene in the zebrafish Danio rerio and the differential response of patched genes to Hedgehog signalling. Dev. Biol. *208*, 14–29.

Liang, Y., Annan, R.S., Carr, S.A., Popp, S., Mevissen, M., Margolis, R.K., and Margolis, R.U. (1999). Mammalian homologues of the Drosophila slit protein are ligands of the heparan sulfate proteoglycan glypican-1 in brain. J. Biol. Chem. *274*, 17885–17892.

Lin, X., Wei, G., Shi, Z., Dryer, L., Esko, J.D., Wells, D.E., and Matzuk, M.M. (2000). Disruption of gastrulation and heparan sulfate biosynthesis in EXT1-deficient mice. Dev. Biol. *224*, 299–311.

Lind, T., Tufaro, F., McCormick, C., Lindahl, U., and Lidholt, K. (1998). The putative tumor suppressors EXT1 and EXT2 are glycosyltransferases required for the biosynthesis of heparan sulfate. J. Biol. Chem. *273*, 26265–26268.

Masai, I., Lele, Z., Yamaguchi, M., Komori, A., Nakata, A., Nishiwaki, Y., Wada, H., Tanaka, H., Nojima, Y., Hammerschmidt, M., et al. (2003). N-cadherin mediates retinal lamination, maintenance of forebrain compartments and patterning of retinal neurites. Development *130*, 2479–2494.

McCormick, C., Duncan, G., Goutsos, K.T., and Tufaro, F. (2000). The putative tumor suppressors EXT1 and EXT2 form a stable complex that accumulates in the Golgi apparatus and catalyzes the synthesis of heparan sulfate. Proc. Natl. Acad. Sci. USA *97*, 668–673.

McFarlane, S., McNeill, L., and Holt, C.E. (1995). FGF signaling and target recognition in the developing *Xenopus* visual system. Neuron *15*, 1017–1028.

McFarlane, S., Cornel, E., Amaya, E., and Holt, C.E. (1996). Inhibition of FGF receptor activity in retinal ganglion cell axons causes errors in target recognition. Neuron *17*, 245–254.

McLaughlin, T., Hindges, R., and O'Leary, D.D. (2003). Regulation of axial patterning of the retina and its topographic mapping in the brain. Curr. Opin. Neurobiol. *13*, 57–69.

Morio, H., Honda, Y., Toyoda, H., Nakajima, M., Kurosawa, H., and Shirasawa, T. (2003). EXT gene family member rib-2 is essential for embryonic development and heparan sulfate biosynthesis in Caenorhabditis elegans. Biochem. Biophys. Res. Commun. *301*, 317–323.

Neff, M.M., Turk, E., and Kalishman, M. (2002). Web-based primer design for single nucleotide polymorphism analysis. Trends Genet. *18*, 613–615.

Nybakken, K., and Perrimon, N. (2002). Heparan sulfate proteoglycan modulation of developmental signaling in Drosophila. Biochim. Biophys. Acta *1573*, 280–291.

Pedersen, L.C., Dong, J., Taniguchi, F., Kitagawa, H., Krahn, J.M., Pedersen, L.G., Sugahara, K., and Negishi, M. (2003). Crystal structure of an α1,4-N-acetylhexosaminyltransferase (EXTL2), a member of the exostosin gene family involved in heparan sulfate biosynthesis. J. Biol. Chem. *278*, 14420–14428.

Picker, A., Brennan, C., Reifers, F., Clarke, J.D., Holder, N., and Brand, M. (1999). Requirement for the zebrafish mid-hindbrain boundary in midbrain polarisation, mapping and confinement of the retinotectal projection. Development *126*, 2967–2978.

Princivalle, M., and de Agostini, A. (2002). Developmental roles of heparan sulfate proteoglycans: a comparative review in Drosophila, mouse and human. Int. J. Dev. Biol. *46*, 267–278.

Ronca, F., Andersen, J.S., Paech, V., and Margolis, R.U. (2001). Characterization of Slit protein interactions with glypican-1. J. Biol. Chem. *276*, 29141–29147.

Schilling, T.F., Piotrowski, T., Grandel, H., Brand, M., Heisenberg, C.P., Jiang, Y.J., Beuchle, D., Hammerschmidt, M., Kane, D.A., Mullins, M.C., et al. (1996). Jaw and branchial arch mutants in zebrafish I: branchial arches. Development *123*, 329–344.

Schlessinger, J., Lax, I., and Lemmon, M. (1995). Regulation of growth factor activation by proteoglycans: what is the role of the low affinity receptors? Cell *83*, 357–360.

Scholes, J.H. (1979). Nerve fibre topography in the retinal projection to the tectum. Nature *278*, 620–624.

Senay, C., Lind, T., Muguruma, K., Tone, Y., Kitagawa, H., Sugahara, K., Lidholt, K., Lindahl, U., and Kusche-Gullberg, M. (2000). The EXT1/EXT2 tumor suppressors: catalytic activities and role in heparan sulfate biosynthesis. EMBO Rep. *1*, 282–286.

Shanmugalingam, S., Houart, C., Picker, A., Reifers, F., Macdonald, R., Barth, A., Griffin, K., Brand, M., and Wilson, S.W. (2000). Ace/Fgf8 is required for forebrain commissure formation and patterning of the telencephalon. Development *127*, 2549–2561.

Steigemann, P., Molitor, A., Fellert, S., Jackle, H., and Vorbruggen, G. (2004). Heparan sulfate proteoglycan syndecan promotes axonal and myotube guidance by slit/robo signaling. Curr. Biol. *14*, 225–230.

Stickney, H.L., Schmutz, J., Woods, I.G., Holtzer, C.C., Dickson, M.C., Kelly, P.D., Myers, R.M., and Talbot, W.S. (2002). Rapid mapping of zebrafish mutations with SNPs and oligonucleotide microarrays. Genome Res. *12*, 1929–1934.

Straznicky, C., Gaze, R.M., and Horder, T.J. (1979). Selection of appropriate medial branch of the optic tract by fibres of ventral retinal origin during development and in regeneration: an autoradiographic study in Xenopus. J. Embryol. Exp. Morphol. *50*, 253–267.

Stuermer, C.A. (1988). Retinotopic organization of the developing retinotectal projection in the zebrafish embryo. J. Neurosci. *8*, 4513–4530.

Takei, Y., Ozawa, Y., Sato, M., Watanabe, A., and Tabata, T. (2004). Three Drosophila EXT genes shape morphogen gradients through synthesis of heparan sulfate proteoglycans. Development *131*, 73–82.

Talbot, W.S., and Schier, A.F. (1999). Positional cloning of mutated zebrafish genes. Methods Cell Biol. *60*, 259–286.

The, I., Bellaiche, Y., and Perrimon, N. (1999). Hedgehog movement is regulated through tout velu-dependent synthesis of a heparan sulfate proteoglycan. Mol. Cell *4*, 633–639.

Toyoda, H., Kinoshita-Toyoda, A., and Selleck, S.B. (2000). Structural analysis of glycosaminoglycans in Drosophila and Caenorhabditis elegans and demonstration that tout-velu, a Drosophila gene related to EXT tumor suppressors, affects heparan sulfate in vivo. J. Biol. Chem. *275*, 2269–2275.

Trowe, T., Klostermann, S., Baier, H., Granato, M., Crawford, A.D., Grunewald, B., Hoffmann, H., Karlstrom, R.O., Meyer, S.U., Muller, B., et al. (1996). Mutations disrupting the ordering and topographic mapping of axons in the retinotectal projection of the zebrafish, Danio rerio. Development *123*, 439–450.

Udin, S.B., and Fawcett, J.W. (1988). Formation of topographic maps. Annu. Rev. Neurosci. *11*, 289–327.

van Eeden, F.J., Granato, M., Schach, U., Brand, M., Furutani-Seiki, M., Haffter, P., Hammerschmidt, M., Heisenberg, C.P., Jiang, Y.J., Kane, D.A., et al. (1996). Genetic analysis of fin formation in the zebrafish, Danio rerio. Development *123*, 255–262.

Walz, A., McFarlane, S., Brickman, Y.G., Nurcombe, V., Bartlett, P.F., and Holt, C.E. (1997). Essential role of heparan sulfates in axon navigation and targeting in the developing visual system. Development *124*, 2421–2430.

Zak, B.M., Crawford, B.E., and Esko, J.D. (2002). Hereditary multiple exostoses and heparan sulfate polymerization. Biochim. Biophys. Acta *1573*, 346–355.

Accession Numbers

The GenBank accession numbers for *ext2* and *extl3* are AY786508 and AY786436, respectively.